

# Determination of the Parameters of the Directivity Pulse Embedded in Near-Fault Ground Motions and Its Effect on Structural Response

Petros Mimoglou, Ioannis N. Psycharis and Ioannis M. Taflampas

**Abstract** Near-fault ground motions are affected by directivity phenomena, which produce important velocity pulses, mostly associated with the normal to the fault direction. Directivity pulses amplify the long period coherent component of the ground motions and are explicitly apparent in the velocity and the displacement time histories and the related response spectra. A number of methods are commonly used for the identification of the parameters of the velocity pulses, mainly their period and amplitude. Also, several mathematical expressions have been proposed for their mathematical representation, which vary from simple functions to more complicated wavelets. A very efficient wavelet is the one proposed by Mavroeidis and Papageorgiou (M&P), which, beyond the period and the amplitude, uses additional parameters related to the total duration and the phase shift of the pulse. In this chapter, a recently proposed new method is presented, which allows the explicit determination of the parameters of the pulse contained in pulse-like records. The M&P wavelet is used for the mathematical representation of the pulse but the proposed methodology can be easily modified to cover other types of wavelets as well. First, the period of the pulse is determined from the peak of the  $S_d \times S_v$  product spectrum, a new concept defined as the product of the velocity and the displacement response spectra. The remaining parameters of the M&P wavelet are derived from the targeted response spectrum of the ground motion applying a relationship that is established between the Cumulative Absolute Displacement (CAD) of a wavelet and its peak spectral amplitude. The method follows a well-defined procedure that can be easily implemented in a computer code for the automatic determination of the pulse parameters of a given ground motion. In the last part of the chapter, the identified pulses, inherent in a wide set of ground motions, are used to study the effect of directivity pulses on the nonlinear response of SDOF structures. It is shown that, in a wide range of periods, the seismic behavior is dominated by the presence of the pulse, since the corresponding M&P wavelet alone can capture quite satisfactorily the nonlinear response.

---

P. Mimoglou · I.N. Psycharis (✉) · I.M. Taflampas  
School of Civil Engineering, Laboratory for Earthquake Engineering,  
National Technical University of Athens, Zografou, Greece  
e-mail: ipsych@central.ntua.gr

## 1 Introduction

The number of recorded near-fault ground motions has increased tremendously in the last decades as a result of denser seismograph stations installed. The plethora of the available records in combination with the use of newer digital instruments, much more capable than the old analog ones, has permitted the identification of important velocity pulses inherent in near-fault ground motions, related to directivity phenomena. These pulses are mostly associated with the normal to the fault direction, and amplify the long period coherent component of the ground motions, explicitly apparent in the velocity and the displacement time histories and the related response spectra.

The identification of the near-fault velocity pulses has instigated further research for the definition of their characteristic parameters, mainly their period and amplitude. Thus, many researchers have presented relations associating the pulse period with the moment magnitude of the event ([1–4] among others).

It should be noted that not all near source ground motions contain directivity pulses, not even all those satisfying the theoretical geometric prerequisites with respect to the rupture geometry. Moreover, although many, if not most, such pulses can be attributed to near-fault effects, it should be pointed out that significant pulses may be produced by other reasons as well, such as basin effects, soil conditions, deep rupture, fling step etc. As noted in the literature [5, 6], long-period record processing can make static displacement due to fling step appear like a directivity pulse.

In this chapter, a new procedure is presented for the determination of the parameters of the velocity pulse inherent in pulse-like ground motions. The proposed methodology can be applied to any record that is *a priori* known to be impulsive, independently of whether it is near-fault or not. The classification of a record as pulse-like or non-pulse-like is an ongoing research field and several researchers have proposed different techniques for this classification (e.g. [7–9]). This issue is beyond the scope of this chapter and is not further discussed in the following; any of the available techniques can be used for this purpose.

The identification of the directivity pulse that is inherent in near-fault ground motions is important in Earthquake Engineering. First, it allows for the generation of artificial time histories compatible with the specific seismic characteristics of each record. Such generation of artificial ground motions with well-defined properties that are consistent with both the physical condition and the characteristics of the actual recorded ground motions is very important in seismic design. Non-linear dynamic structural analyses generally require the use of large numbers of input ground motions in order to determine the performance of structures, while the number of available recorded ground motions is limited and scaling of existing records is not appropriate in most cases. In general, according to the usual practice for the generation of synthetic ground motions with forward directivity effects, the frequency content of the eventual time histories can be divided in two components: (a) the high-frequency incoherent component of the ground motion, which is

typically generated using stochastic procedures accounting for the distribution of the seismic moment on the fault plane, as the ones proposed in [10–12]; and (b) the low-frequency coherent component, which is associated with the pulse inherent in the ground motion. Mavroeidis and Papageorgiou [13] proposed a method to combine the two components, which requires the selection of a proper scenario based on the statistical characteristics of a dataset for both components. This method has been applied in [14–16] for the analysis of different engineering problems.

Second, it allows for a better selection and scaling of records to be used for linear and nonlinear analyses. It is known that pulse-like ground motions account for large spectral values at periods close to the pulse period [17], while the  $R_y - \mu$  relation diverts from unity for periods smaller than half the pulse period [18].

Due to the importance of the velocity pulses for the linear and the nonlinear response of the structures, several mathematical expressions have been proposed for their representation. These models vary from simple functions to more complicated wavelets like the Daubechies wavelet [10] used in [5, 7, 17, 19]. A very efficient wavelet was proposed by Mavroeidis and Papageorgiou [13], who introduced additional parameters regarding the total duration and the phase shift of the pulse.

In the new method presented herein, the efficient Mavroeidis and Papageorgiou wavelet, referred as M&P wavelet hereafter, is used for the pulse representation. Up to now, the properties of the M&P wavelet were determined either with a trial and error procedure, as in the original paper [13], or through a wavelet analysis, as the one proposed in [20]. The new procedure is based on the displacement—velocity product spectrum ( $S_d \times S_v$ ), which is used for the identification of the period of the pulse, and a relation between the ground motion parameter  $CAD$  (Cumulative Absolute Displacement [21]) and the peak of the displacement response spectrum, which is used for the determination of the remaining parameters of the wavelet.

## 2 Determination of the Parameters of the Directivity Pulse

### 2.1 Determination of the Period, $T_p$

The period  $T_p$  of the directivity pulse embedded in near-fault ground motions is the most important parameter and has attracted the attention of several researchers who have presented regression relationships associating its value with the moment magnitude of the event ([1–4] among others). As a common practice, it is usually determined from the peak of the pseudo-velocity response spectrum for 5 % damping. However, the accuracy of this definition has been questioned [7, 22].

An example in which this definition leads to false results is shown in Fig. 1 for the normal to the fault component of the Petrolia record of the Cape Mendocino, 1992 earthquake. In Fig. 1a, the time history of the ground velocity is shown; the motion is characterized by a pulse of period 2.74 s, as evident from the red line

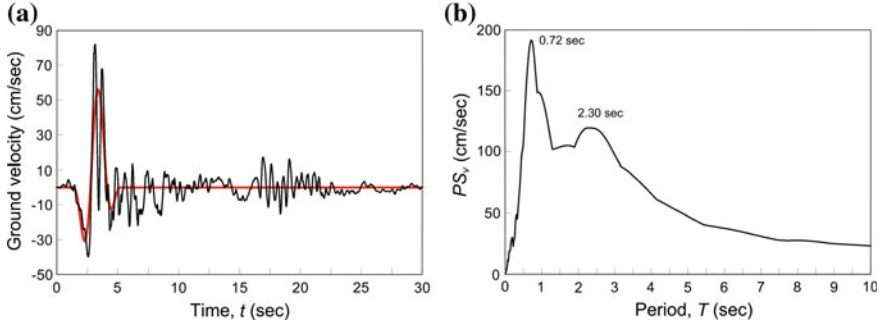


**Fig. 1** Normal to the fault component of the Petrolia record of the Cape Mendocino, 1992 earthquake: **a** time history of ground velocity; **b** pseudo-velocity response spectrum for 5 % damping. Red line shows the directivity pulse determined with the methodology presented herein

which corresponds to the wavelet identified with the procedure presented in the following. This value is similar to the pulse period  $T_p = 3.0$  s calculated by Baker [7]. However, the period that corresponds to the largest peak of the pseudo-velocity response spectrum for 5 % damping is equal to 0.72 s (Fig. 1b), while a peak of significantly smaller amplitude appears at  $T = 2.3$  s.

An alternative to the calculation of  $T_p$  from the pseudo-velocity response spectrum would be to use the displacement response spectrum instead. This consideration comes from the fact that the displacement response spectrum is an adequate envelope curve of the Fourier amplitude spectrum of the ground velocity, similarly with the undamped velocity response spectrum which is an envelope of the Fourier amplitude spectrum of the ground acceleration. Indeed, as proven by Hudson [23]:

$$\tilde{a}_g(\omega) \leq S_{v,0}(\omega) \quad (1)$$

where  $\tilde{a}_g(\omega)$  is the Fourier spectrum amplitude of the ground acceleration  $a_g(t)$ , defined by

$$\tilde{a}_g(\omega) = \sqrt{\left[ \int_0^{t_{tot}} a_g(t) \cdot \cos(\omega t) dt \right]^2 + \left[ \int_0^{t_{tot}} a_g(t) \cdot \sin(\omega t) dt \right]^2} \quad (2)$$

$t_{tot}$  being the duration of the ground motion, and  $S_{v,0}(\omega)$  is the velocity response spectrum for zero damping.

Similarly, it can be proven that the undamped displacement response spectrum is an adequate envelope of the Fourier spectrum of the ground velocity. Indeed, for undamped oscillators ( $\xi = 0$ ) one can assume that the velocity response spectrum,  $S_{v,0}(\omega)$ , coincides with the pseudo-velocity one,  $PS_{v,0}(\omega)$ , except in the long period range. Thus, in a wide range of periods, it can be assumed that  $S_{v,0}(\omega) \approx$

$\omega \cdot S_{d,0}(\omega)$ , where  $S_{d,0}(\omega)$  is the displacement response spectrum for zero damping. Then, dividing both sides of relation (1) by  $\omega$  and taking under consideration that  $\tilde{a}_g(\omega)/\omega = \tilde{v}_g(\omega)$ , where  $\tilde{v}_g(\omega)$  is the Fourier amplitude spectrum of the ground velocity,  $v_g(t)$ , determined by

$$\tilde{v}_g(\omega) = \sqrt{\left[ \int_0^{t_{tot}} v_g(t) \cdot \cos(\omega t) dt \right]^2 + \left[ \int_0^{t_{tot}} v_g(t) \cdot \sin(\omega t) dt \right]^2} \quad (3)$$

one gets:

$$\tilde{v}_g(\omega) \leq S_{d,0}(\omega) \quad (4)$$

which shows that the displacement response spectrum is an adequate envelope curve of the Fourier amplitude spectrum of the ground velocity. An example is shown in Fig. 2a for the normal to the fault component of the Petrolia record of the Cape Mendocino, 1992 earthquake.

Based on the above observation, and taking under consideration that the directivity pulse is prominent in the time history of the ground velocity, it would be reasonable to determine its period,  $T_p$ , from the predominant period of the displacement response spectrum. For the Petrolia record, this definition leads to  $T_p = 2.67$  s (Fig. 2b), which is close to the period of the pulse (2.74 s) that can be identified in the ground velocity record using the methodology presented herein (Fig. 1a).

This alternative definition of the pulse period,  $T_p$ , however, through the predominant period of the displacement response spectrum, might be problematic, as the peak of the displacement response spectrum can be affected by the presence of

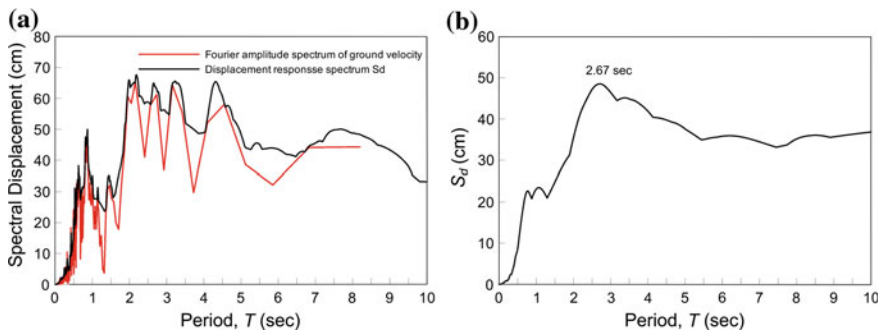


**Fig. 2** Normal to the fault component of the Petrolia record of the Cape Mendocino, 1992 earthquake: **a** Comparison of the Fourier amplitude spectrum of the ground velocity with the displacement response spectrum for zero damping; **b** displacement response spectrum for 5 % damping

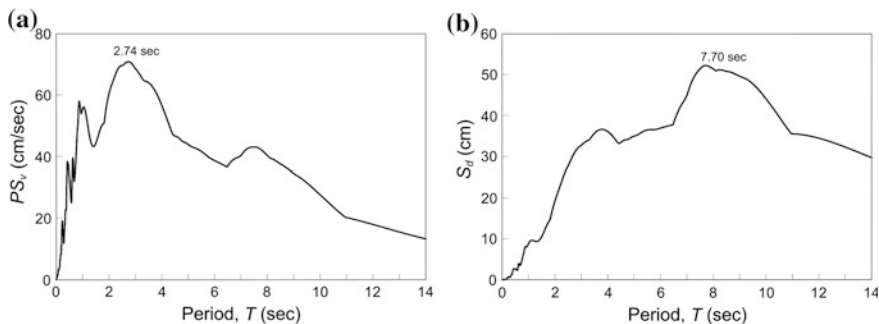


**Fig. 3** Normal to the fault component of the Parachute Test Site record of the Westmorland, 1981 earthquake: **a** pseudo-velocity response spectrum for 5 % damping; **b** displacement response spectrum for 5 % damping

long period errors in the ground acceleration record. Furthermore, the peak of the displacement response spectrum may correspond to a velocity pulse with large area but small amplitude, which might not be the prevailing pulse. In addition, it cannot be generalized either, as there are cases in which it is not valid. An example is given in Fig. 3 for the normal to the fault component of the ground motion recorded at Parachute Test Site during the Westmorland, 1981 earthquake. In this case, the period of the directivity pulse,  $T_p$ , is equal to 3.6 s according to Baker [7] and to 3.0 s according to the method presented herewith, values which are close to the predominant period of the pseudo-velocity response spectrum (Fig. 3a) and not to the predominant period of the displacement response spectrum which is quite larger, equal to 7.70 s (Fig. 3b).

As evident from the above discussion, neither the pseudo-velocity nor the displacement response spectra can be generally used for the determination of the period of the directivity pulse, since there are cases in which the two approaches lead to significantly different results. This happens because many near-fault ground motions are affected by more than one pulses of different period. Herein, a new methodology is proposed which allows the identification of the predominant pulse that is related to directivity phenomena of near-fault ground motions through a combination of the velocity and the displacement response spectra.

Specifically, since the pulse-like components of near-fault ground motions affect both the ground acceleration and the ground velocity, although to a different degree, the pulse period,  $T_p$ , should prevail in the convolution integral of these two time histories. Furthermore, extreme high or low frequency components inherent in the ground acceleration and the ground velocity are attenuated. Consequently, the peak of the acceleration—velocity convolution should correspond to the period of the predominant pulse contained in the ground motion.

It is known that the Fourier spectrum of the convolution integral is equal to the product of the Fourier spectra of the convolved signals. On the other hand, as mentioned above, the undamped velocity spectrum,  $S_{v,0}$ , is an envelope of the

Fourier amplitude spectrum of the ground acceleration and the undamped displacement spectrum,  $S_{d,0}$ , is an envelope of the Fourier spectrum of the ground velocity. Using these properties, the Fourier spectrum of the convolution integral can be approximated by the product  $S_{v,0} \times S_{d,0}$ , which in the following will be referred as the *product spectrum for zero damping*. Accordingly, the period of the directivity pulse can be determined from the peak of the product spectrum.

As mentioned above, this conclusion is justified for the product spectrum for zero damping. However, it can be extended to the product spectrum for 5 % damping, which is defined as the product  $S_{v,5} \times S_{d,5}$ , where  $S_{v,5}$  and  $S_{d,5}$  are the velocity and displacement response spectra for 5 % damping, respectively, since the period at which the  $S_{v,5} \times S_{d,5}$  product spectrum peaks is expected to be close to the one at which the  $S_{v,0} \times S_{d,0}$  product spectrum peaks. Although these periods do not necessarily coincide, it is suggested here to use the spectra for 5 % damping for the calculation of the pulse period for the following reasons:

- Because the results match better the periods derived by Baker [7], which are used here as benchmark data.
- Because the response spectra of the ground motion for 5 % damping, which are more important than the ones for zero damping for typical earthquake engineering applications, are matched better by the corresponding spectra of the extracted velocity pulses. The procedure presented herein for the determination of the parameters of the directivity pulse is based on the best fitting of the response spectrum for 5 % damping.
- Because it is consistent with the above-mentioned current practice of calculating the pulse period from the pseudo-velocity response spectrum for 5 % damping; however, this cannot serve as an argument in favor of using spectra for 5 % damping, due to the above-mentioned shortcomings of this method.

In the following, only the spectra for 5 % damping will be used, denoted as  $S_d$  and  $S_v$  without further reference to the damping value. Thus, the  $S_d \times S_v$  product spectrum will denote the  $S_{v,5} \times S_{d,5}$  product.

The application of the new method for the calculation of the pulse period,  $T_p$ , is presented in Fig. 4 for the above-mentioned records, namely the normal to the fault components of the Petrolia record and the Parachute Test Site record. As mentioned above, in the former case, the pulse period was calculated to  $T_p = 3.0$  s by Baker [7] and is associated with the predominant period of the displacement response spectrum (Fig. 2); in the latter, it was calculated to  $T_p = 3.6$  s by Baker and is associated with the predominant period of the pseudo-velocity response spectrum (Fig. 3). The use of the  $S_d \times S_v$  product spectrum allows for the correct calculation of the pulse period in both cases, namely,  $T_p = 2.74$  s and 3.00 s, respectively.

In Fig. 4, the corresponding product spectra for zero damping are also presented for comparison. It is noted that the selection of the appropriate peaks in this case is somehow uncertain and might lead to different results.

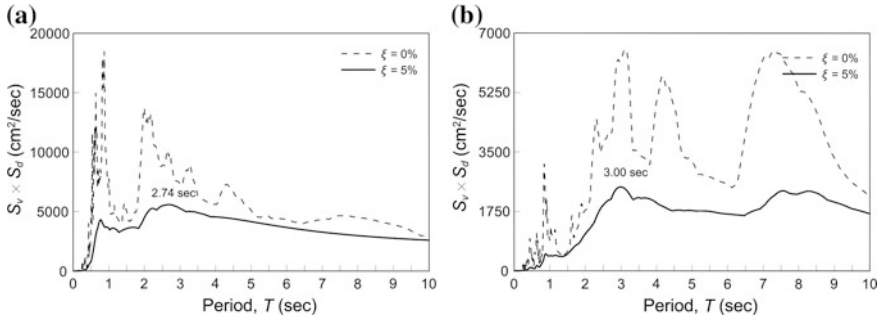


**Fig. 4** Determination of the velocity pulse period,  $T_p$ , from the peak of the  $S_d \times S_v$  product spectrum for 5 % damping (the corresponding curves for zero damping are also shown for comparison): **a** normal to the fault component of the Petrolia record of the Cape Mendocino, 1992 earthquake; **b** normal to the fault component of the Parachute Test Site record of the Westmorland, 1981 earthquake

## 2.2 Pulse Determination

### 2.2.1 Mathematical Representation of the Pulse

The proposed methodology is based on a wavelet representation of the directivity pulse, the period of which is identified from the peak of the convolution spectrum for 5 % damping, as explained in the previous section. For the mathematical representation of the pulse, the wavelet proposed by Mavroeidis and Papageorgiou [13] (M&P wavelet) is adopted. However, one could modify the proposed methodology appropriately to consider other well-known wavelets proposed in the literature.

The M&P wavelet is derived by the coupling of a harmonic oscillation signal and a bell-shaped envelope. Four parameters are used to define the pulse:

- The period  $T_p$  of the harmonic oscillation of the wavelet.
- The amplitude  $A$  of the bell-shaped envelope, which is associated with the amplitude of the time history of the velocity.
- The duration  $\gamma$  of the wavelet, which measures the number of the oscillations and is defined as  $\gamma = t_{tot}/T_p$  with  $\gamma > 1$ ,  $t_{tot}$  being the time duration of the wavelet.
- The phase shift  $\nu$ .

The duration of the ground motion affects the response of the structures and especially the response spectrum amplification. The phase angle controls the shape of the wavelet, which, thus, can best fit the velocity time history. The importance of the number of cycles and the phase modulation of the wavelets on their capability to match pulse-like ground motions was reported by Vassiliou and Makris [20].



The use of the above-mentioned four parameters gives the M&P wavelet additional flexibility compared to simpler models, enabling it to better approximate more complex velocity pulses. Additionally, it has a closed form solution, which makes it easier to use and study. The ability of the M&P wavelet to capture satisfactorily the effects of the base excitation characteristics on the response has made it popular for the representation of pulse-like ground motions for engineering purposes and several researchers have used it for linear and nonlinear analyses ([14–16] among others). Due to these advantages, and since the proposed methodology is spectrum oriented, the M&P wavelet was selected among other widely used wavelets, the parameters of which are not directly related to the structural response, as for example the Daubechies wavelet [24] used by Baker [7] for the identification of the predominant pulse.

Using the above-mentioned parameters, the acceleration  $a_p(t)$  and the velocity  $v_p(t)$  of the wavelet can be defined by the following equations [13]:

$$a_p(t) = \begin{cases} -\frac{A\pi}{\gamma T_p} \left[ \sin\left(\frac{2\pi}{\gamma T_p}(t - t_0)\right) \cdot \cos\left(\frac{2\pi}{T_p}(t - t_0) + v\right) \right. \\ \left. + \gamma \cdot \sin\left(\frac{2\pi}{T_p}(t - t_0) + v\right) \cdot \left[1 + \cos\left(\frac{2\pi}{\gamma T_p}(t - t_0)\right)\right] \right], & t_0 - \frac{\gamma}{2}T_p \leq t \leq t_0 + \frac{\gamma}{2}T_p \\ 0, & \text{otherwise} \end{cases} \quad (5)$$

$$v_p(t) = \begin{cases} \frac{A}{2} \left[1 + \cos\left(\frac{2\pi}{\gamma T_p}(t - t_0)\right)\right] \cdot \cos\left(\frac{2\pi}{T_p}(t - t_0) + v\right), & t_0 - \frac{\gamma}{2}T_p \leq t \leq t_0 + \frac{\gamma}{2}T_p \\ 0, & \text{otherwise} \end{cases} \quad (6)$$

where  $t_0$  is the time defining the epoch of the envelope's peak.

In the methodology presented herewith, the parameters of the wavelet are determined by best fitting the displacement response spectrum. However, since the pseudo-velocity response spectrum is directly related to the displacement spectrum through the relation  $PS_v = \omega \cdot S_d$ , the derived wavelet will also fit the pseudo-velocity response spectrum.

Having determined the period,  $T_p$ , of the pulse from the peak of the  $S_d \times S_v$  product spectrum as described in the previous section, the determination of the three remaining parameters of the wavelet,  $A$ ,  $\gamma$  and  $v$ , is achieved with the use of the recently proposed ground motion index *CAD* (Cumulative Absolute Displacement [21]) and a cross correlation operation between the proposed wavelet and the record time history. *CAD* is defined by the time integral of the absolute ground velocity, in analogy with the *CAV* index (Cumulative Absolute Velocity [25]), i.e.

$$CAD = \int_0^{t_{tot}} |v_g(t)| dt \quad (7)$$

It is noticed that Baker [7] and Zamora and Riddell [26] have also used similar indices, specifically the time integral of the squared acceleration [27] and the time integral of the squared velocity [22], as intensity measures of the pulse-like content of the ground motion.

### 2.2.2 Determination of the Amplitude, $A$

Let us consider a harmonic ground motion of amplitude  $d_{g,\max}$ , which is applied as base excitation to an undamped SDOF oscillator. At resonance, the amplitude of the response of the oscillator builds up almost linearly with the number of cycles and for an excitation of  $\gamma$  cycles the maximum response is [28]:

$$S_{d,0}(T_{res}) = \pi \gamma d_{g,\max} \quad (8)$$

in which  $S_{d,0}(T_{res})$  denotes the spectral displacement at resonance for zero damping. On the other hand, the value of  $CAD$  at the end of the  $\gamma$ th cycle of a harmonic excitation is:

$$CAD = 4 \gamma d_{g,\max} \quad (9)$$

Therefore, for a harmonic excitation of  $\gamma$  cycles there is a constant relation between the spectral displacement for zero damping at resonance and  $CAD$ , which can be expressed as

$$\frac{S_{d,0}(T_{res})}{CAD} = \frac{\pi}{4} \quad (10)$$

If an M&P wavelet is used instead of the purely harmonic excitation, Eqs. (8) and (10) continue to hold approximately, with satisfactory accuracy, despite the fact that the bell-shaped envelope has been applied to the amplitude of the excitation. This is shown in Fig. 5a, in which the ratio of the maximum spectral displacement

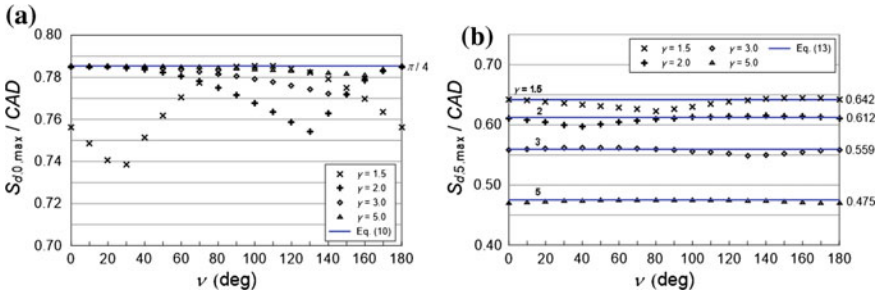


**Fig. 5** Relation between the peak spectral displacement  $S_{d,\max}$  and  $CAD$  for M&P wavelets with various values of  $\gamma$  and  $\nu$ : **a** zero damping; **b** 5% damping

for zero damping over the cumulative absolute displacement,  $S_{d,0,\max}/CAD$ , is plotted versus the phase index  $\nu$  for  $\gamma = 1.5, 2.0, 3.0$  and  $5.0$ . The results are independent of the period  $T_p$  and the amplitude  $A$ . It is evident that the ratio  $S_{d,0,\max}/CAD$  is close to the value  $\pi/4$ , which holds for harmonic excitations according to Eq. (10), especially for pulses of long duration (large values of  $\gamma$ ). The largest discrepancy occurs for  $\gamma = 1.5$  and  $\nu = 30^\circ$ , but even in that case the error is less than 6 % (lowest value is about 0.74 compared to  $\pi/4 = 0.785$ ).

A similar relation between the peak spectral displacement and  $CAD$  can also be established for other values of damping, apart from zero. For a SDOF oscillator of damping equal to  $\xi$  and for purely harmonic excitation, the displacement at resonance is [28]:

$$S_{d,\xi}(T_{res}) = \frac{1 - e^{-2\pi\gamma\xi}}{2\xi} \cdot d_{g,\max} \quad (11)$$

Using again Eq. (9), the following relation can be established:

$$\frac{S_{d,\xi}(T_{res})}{CAD} = \frac{1 - e^{-2\pi\gamma\xi}}{8\gamma\xi} \quad (12)$$

If the excitation is not purely harmonic but an M&P wavelet, Eq. (12) produces an error for large values of  $\gamma$ . A parametric investigation that was performed showed that a correction factor must be applied in this case, equal to  $1 + (\gamma-1)\xi$ . Thus, for M&P wavelets, the following relation applies:

$$\frac{S_{d,\xi,\max}}{CAD} = \frac{1 - e^{-2\pi\gamma\xi}}{8\gamma\xi} [1 + (\gamma - 1)\xi] \quad (13)$$

Comparison of the values produced by Eq. (13) with the actual values of the ratio  $S_{d,\xi,\max}/CAD$ , obtained for various values of  $\nu$  and  $\gamma$ , is shown in Fig. 5b for  $\xi = 5\%$ . It is evident that the accuracy obtained with Eq. (13) is very satisfactory in all cases.

Using Eqs. (10) and (12) and the well-known relation between spectral displacement and pseudo-spectral velocity:  $PS_v = (2\pi/T) \cdot S_d$ , the following relations can be established between  $CAD$  and  $PS_v$  for M&P wavelets:

$$\frac{PS_{v,0,\max}}{CAD} = \frac{\pi^2}{2T_p} \quad \text{for zero damping} \quad (14)$$

$$\frac{PS_{v,\xi,\max}}{CAD} = \frac{\pi(1 - e^{-2\pi\gamma\xi})[1 + (\gamma - 1)\xi]}{4\gamma\xi T_p} \quad \text{for damping } \xi \neq 0 \quad (15)$$

in which  $PS_{v,0}$  and  $PS_{v,\xi}$  denote the pseudo-spectral velocity for zero damping and damping equal to  $\xi$ , respectively.

For M&P wavelets, the value of  $CAD$  is directly associated with the amplitude  $A$  and the duration index  $\gamma$ , since the following relation holds:

$$CAD = \gamma A T_p / \pi \quad (16)$$

As already mentioned, the new method is spectrum oriented and the directivity pulse is defined to best fit the response spectrum of the original record. In this sense, substituting  $CAD$  in Eqs. (14) and (15) using (16) one gets:

$$A = \frac{2PS_{v,0}(T_p)}{\pi \gamma} \quad \text{for zero damping} \quad (17)$$

$$A = \frac{4 \xi PS_{v,\xi}(T_p)}{(1 - e^{-2\pi\gamma\xi}) \cdot [1 + (\gamma - 1)\xi]} \quad \text{for damping } \xi \neq 0 \quad (18)$$

in which  $PS_{v,0}(T_p)$  and  $PS_{v,\xi}(T_p)$  are the values of the pseudo-velocity response spectrum of the ground motion for zero damping and damping equal to  $\xi$ , respectively, calculated for period  $T_p$ . As mentioned above, the displacement response spectrum can be used instead of the pseudo-velocity one, since  $PS_v(T_p) = (2\pi/T_p) \cdot S_d(T_p)$ .

Among Eqs. (17) and (18), Eq. (18) is preferred for the determination of the amplitude  $A$  because the produced wavelet matches better the spectra for the desired value of damping. Typically, the pseudo-velocity spectrum for 5 % damping is used, thus Eq. (15) is usually applied for  $\xi = 0.05$ . However, Eq. (17) should be used in case that one wants to calibrate the wavelets with the response spectrum for zero damping.

### 2.2.3 Determination of the Duration, $\gamma$ , and Phase Shift, $\nu$

For the determination of the wavelet's amplitude,  $A$ , from Eq. (18), the value of the duration,  $\gamma$ , must be known. Since this is an unknown parameter, all the values in a selected range of variation of  $\gamma$  are examined.

From this set of pairs  $(A, \gamma)$ , the ones that lead to amplitudes of the wavelet's acceleration, velocity or displacement larger than the corresponding peak values of the ground motion, namely the peak ground acceleration,  $pga$ , the peak ground velocity,  $pgv$  and the peak ground displacement,  $pgd$ , respectively, are rejected.

For the remaining acceptable pairs  $(A, \gamma)$ , and for all values of the phase,  $\nu$ , between  $0^\circ$  and  $360^\circ$ , the corresponding wavelets are calculated. For each of these wavelets, several values of time delay,  $t_d$ , for the initiation of the pulse are examined. Thus, a set of candidate wavelets is determined, each one corresponding to a different set of parameters  $A$ ,  $\gamma$ ,  $\nu$  and  $t_d$ .

From the corresponding pulse time histories,  $v_p(A, \gamma, \nu, t_d, t)$ , the wavelet that correlates best with the time history of the ground velocity,  $v_g(t)$ , is selected. To this

end, the cross correlation factor,  $r$ , is calculated for each pair of time histories ( $v_p$ ,  $v_g$ ) and the pulse with the largest  $r$  is selected.

It is reminded that the cross-correlation operation between two functions  $f$  and  $g$  with a time delay  $t_d$  is defined by

$$(f * g)(t_d) = \int_{-\infty}^{\infty} f^*(t) \cdot g(t + t_d) dt \quad (19)$$

where  $f^*$  is the complex conjugate of  $f$ . The cross-correlation factor  $r$  is defined by

$$r = \frac{\sum_i (f(t_i) - \tilde{f}) \cdot (g(t_i - t_d) - \tilde{g})}{\sqrt{\left[ \sum_i (f(t_i) - \tilde{f})^2 \right] \cdot \left[ \sum_i (g(t_i - t_d) - \tilde{g})^2 \right]}} \quad (20)$$

where  $\tilde{f}$  and  $\tilde{g}$  are the mean values of the functions  $f$  and  $g$  respectively.

In this way, the cross correlation operation is used to identify not only the pulse which best fits the velocity time history of the ground motion, but also its starting time,  $t_d$ . It is mentioned that the time delay,  $t_d$ , is related to  $t_0$  defining the epoch of the envelope's peak of the wavelet [see Eqs. (5) and (6)] through the equation:

$$t_d = t_0 - \gamma T_p / 2. \quad (21)$$

### 2.3 The Method in Steps

Based on the aforementioned theoretical background, a straightforward procedure can be established for the determination of the significant pulse and its parameters in terms of the corresponding M&P wavelet. The method, which can be implemented easily in a computer code, consists of the following steps:

- Step 1 For the ground motion under consideration produce the  $S_d \times S_v$  product spectrum by multiplying the displacement and the pseudo-velocity response spectra for 5 % damping.
- Step 2 Identify the period that corresponds to the largest peak of the  $S_d \times S_v$  product spectrum and set  $T_p$  equal to this value. Calculate the value of  $PS_{v,5}(T_p)$  from the corresponding value of the pseudo-velocity response spectrum for  $\xi = 5$  %.
- Step 3 Set a maximum value,  $\gamma_{\max}$ , for the duration of the M&P wavelet. As the duration of the wavelet is not known a priori, a sweep of all possible values of  $\gamma$  between 1 and  $\gamma_{\max}$  is needed for the determination of the most suitable wavelet for the specific ground motion. For directivity pulses of near fault ground motions,  $\gamma_{\max} = 5$  is usually adequate. In some cases, however, larger values of  $\gamma_{\max}$  are required, up to  $\gamma_{\max} = 10$

or even larger. A step of  $\Delta\gamma = 0.1$  is suggested to be used for the determination of the values of  $\gamma$  during the sweep process.

For each  $\gamma_i$  in the range  $1 \leq \gamma_i \leq \gamma_{\max}$  with step  $\Delta\gamma$  and for the value of  $PS_{v,5}(T_p)$  that was determined in step 2 define the corresponding value of the wavelet amplitude,  $A_i$ , using Eq. (18) for  $\xi = 0.05$ .

- Step 4 For each pair  $(A_i, \gamma_i)$  that was determined in step 3 and for values of the phase  $\nu$  ranging from  $0^\circ$  to  $360^\circ$  produce the corresponding M&P wavelet using Eqs. (5) and (6) leaving  $t_0$  as a parameter. A step of  $\Delta\nu = 5^\circ$  is suggested to be used for the sweep of the phase shift. Reject all the wavelets for which the peak acceleration or the peak velocity or the peak displacement is larger than the corresponding values of the ground motion,  $pga$ ,  $pgv$  and  $pgd$ , respectively.
- Step 5 For the remaining wavelets, each one corresponding to an acceptable value of  $\gamma$ , and for all values of  $t_0$  ranging from  $t_0 = \gamma_i T_p/2$  to  $t_0 = t_{\max} - \gamma_i T_p/2$ , with  $t_{\max}$  being the total duration of the record, calculate the corresponding correlation factor  $r_i$  between the velocity time history of each wavelet,  $v_{p,i}(t)$ , and the time history of the original ground velocity,  $v_g(t)$ , and the time delay  $t_{d,i}$  using Eqs. (20) and (21). Choose the wavelet with the largest cross correlation factor  $r$  and define  $A$ ,  $\gamma$ ,  $\nu$  and  $t_0$  from the parameters of this wavelet. Calculate the start time of the pulse from Eq. (21). It must be noted that, if the correlation factors for the selected wavelets are quite low, it is questionable whether the ground motion under consideration can be considered as a pulse-like one.

## 2.4 Example

As an example, the new method is applied to the Gebze record of the Kocaeli, Turkey, 1999 earthquake. The normal to the fault component of this record, as provided in [29], is used.

- Step 1 First, the  $S_d \times S_v$  product spectrum of the record is derived as the product of the velocity and the displacement response spectra for 5 % damping (Fig. 6c, solid line).
- Step 2 The peak of the  $S_d \times S_v$  spectrum corresponds to  $T_p = 4.88$  s. It is noted that the corresponding spectrum for zero damping (Fig. 6a, dashed line) peaks at a much larger period, specifically  $T = 9.06$  s. However, according to the proposed procedure, the pulse period is assigned to the peak of the  $S_d \times S_v$  product spectrum for 5 % damping, thus the pulse period is set to:  $T_p = 4.88$  s. The corresponding pseudo-velocity spectral value is  $PS_{v,5}(T_p) = 95.19$  cm/s (Fig. 6d). Note that this value does not correspond to a peak of the pseudo-velocity spectrum; in general, however, it is close to a local peak if not to the largest peak.

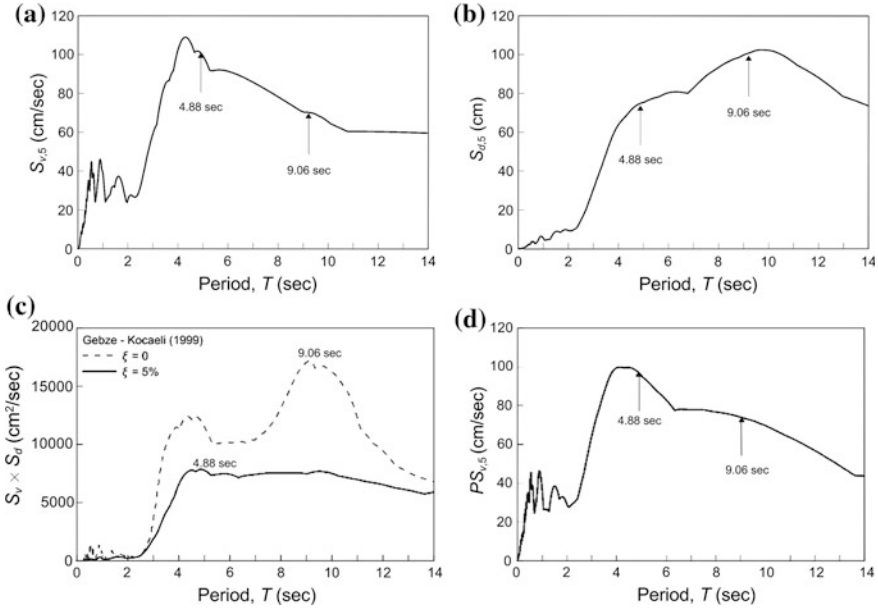


**Fig. 6** Normal to the fault component of the Gebze record of the Kocaeli, Turkey, 1999 earthquake: **a**  $S_v$  for 5 % damping; **b**  $S_d$  for 5 % damping; **c**  $S_d \times S_v$  product spectra for 5 % damping (solid line) and zero damping (dashed line); **d** pseudo-velocity response spectrum for 5 % damping

Step 3 In this example,  $\gamma_{\max}$  is set to 5 and the amplitude,  $A$ , is derived for each  $\gamma$  in the range  $1 \leq \gamma \leq 5$  with step  $\Delta\gamma = 0.1$  using Eq. (18).

Step 4 For each pair  $(A, \gamma)$ , and for values of the phase,  $\nu$ , ranging from  $0^\circ$  to  $360^\circ$  with step  $\Delta\nu = 5^\circ$ , the corresponding M&P wavelet is determined for  $T_p = 4.88$  s and leaving  $t_0$  as a parameter. Since for the record under consideration  $pga = 233.73$  cm/s<sup>2</sup>,  $pgv = 51.97$  cm/s and  $pgd = 44.09$  cm, all wavelets with peak acceleration larger than 233.73 cm/s<sup>2</sup> or peak velocity larger than 51.97 cm/s or peak displacement larger than 44.09 cm are rejected.

Step 5 For the remaining wavelets and for all values of  $t_0$  ranging from  $t_0 = \gamma_i \cdot T_p/2$  to  $t_0 = t_{\max} - \gamma_i \cdot T_p/2$ , with  $t_{\max} = 28$  s being the total duration of the record, the cross correlation factor,  $r$ , is calculated between the velocity time history of each wavelet and the time history of the original ground velocity. The wavelet with the largest cross correlation factor is chosen to represent the velocity pulse. In this example, the characteristics of the chosen wavelet are:  $A = 42.18$  cm/s,  $\gamma = 1.8$ ,  $\nu = 190^\circ$  and  $t_0 = 7.76$  s. The start time of the velocity pulse is:  $t_d = 7.76 - 1.8 \times 4.88/2 = 3.37$  s.

Comparison of the time histories (acceleration and velocity) of the extracted pulse with those of the original record is shown in Fig. 7a,

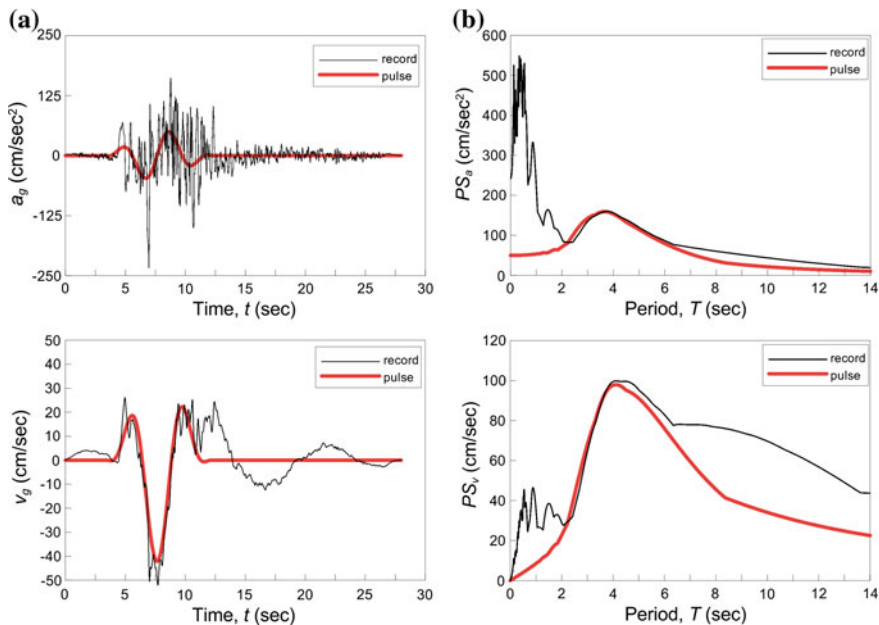


**Fig. 7** Normal to the fault component of the Gebze record of the Kocaeli, Turkey, 1999 earthquake: **a** Comparison of the acceleration and velocity time histories of the chosen M&P wavelet (red line) with the ones of the original record (black line); **b** comparison of the corresponding response spectra for 5 % damping

while the comparison of the corresponding response spectra for 5 % damping is depicted in Fig. 7b. It is seen that the selected pulse can capture very well both the time histories of the velocity pulse inherent in the ground motion and the response spectra of the original record in the period regime around the pulse period.

### 3 Calculation of Additional Important Pulses

In many near-fault records there are additional significant pulses inherent in the ground motion. In fact, as Mavroeides and Papageorgiou [13] and others have noted, there are cases in which more than one pulses are required to capture the nature of the phenomenon. In order to identify the additional pulses, apart from the predominant one, the proposed methodology can also be used, if applied to the *residual ground motion* instead of the original record. The residual ground motion is derived by subtracting the wavelet that was defined in step 5 of the above-mentioned procedure from the original record. The resulting record is considered as a *new ground motion* to which the methodology for the identification of the significant pulse can be applied. This procedure can be repeated until all the



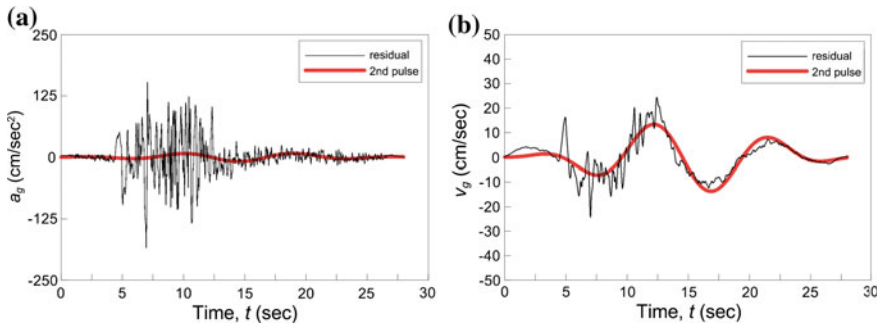


**Fig. 8** Significant pulse embedded in the *residual* ground motion of the Gebze record after subtraction of the pulse of Fig. 7a: Comparison of **a** the acceleration and **b** the velocity time histories of the pulse and the residual record

significant pulses are identified. Note that other researchers (e.g. Shahi [19]) have used their own methods to extract multiple pulses.

It should be mentioned that, although this process will identify additional pulses, it lacks a criterion to judge if the detected pulses are, in fact, primary characteristics of the ground motion. Several criteria have been proposed for the characterization of pulses as significant and the interested reader may refer to the bibliography. This issue exceeds the scope of this chapter and is not further discussed in the ensuing.

As an example, the proposed method is applied to the normal to the fault component of the Gebze record of the Kocaeli, Turkey, 1999 earthquake, for which the first significant pulse was determined previously (Sect. 2.4). This pulse is subtracted from the original ground motion and the *residual motion* is calculated, which is used for the identification of the second pulse. Application of steps 1–5 to the residual record ends up with the second pulse which is shown in Fig. 8.

Adding the two pulses, a *combined* pulse is derived, which provides a better approximation to the original record. This is shown in Fig. 9 (top row), where the time histories of the original record are compared with the time histories of the combined pulse. The corresponding response spectra are compared in the bottom row of Fig. 9.

## 4 Effect of the Directivity Pulse on the Inelastic Response

The existence of the directivity pulse in the ground motion has an important effect on the response of the structures. In what regards the elastic response, it is known that it produces a bell shaped amplification to the acceleration response spectrum, centered around the pulse period (Shahi and Baker [17]). This spectral amplification, if measured as the ratio of the spectral acceleration corresponding to the time history containing the pulse over the spectral acceleration corresponding to the time history of the residual ground motion after the extraction of the pulse, attains values

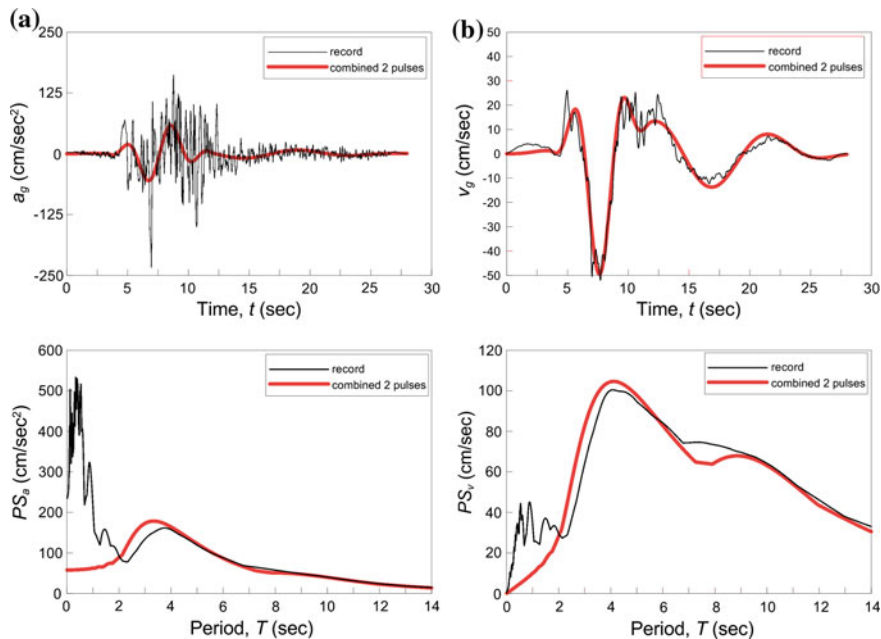


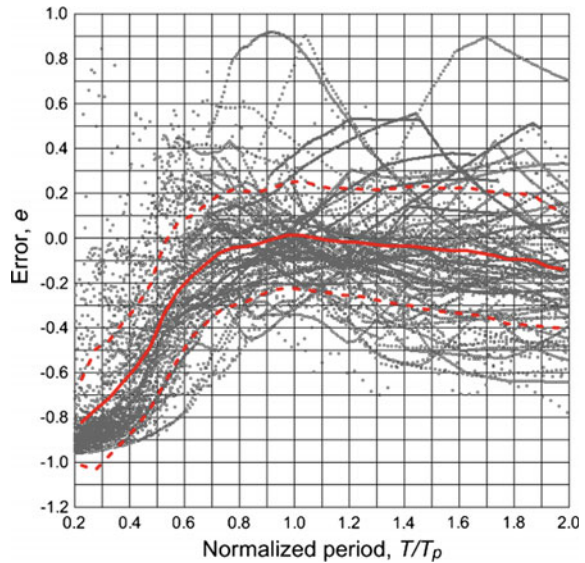
**Fig. 9** Normal to the fault component of the Gebze record of the Kocaeli, Turkey, 1999 earthquake: comparison of **a** the acceleration and **b** the velocity time histories (*top row*) and corresponding response spectra (*bottom row*) of the *combined* pulse, composed of the superposition of the two first detected significant pulses, and the original record

of about 3 in the average, while its maximum value can be as large as 5–6. This means that, if directivity phenomena are ignored, the design spectral accelerations, as given by modern design codes, can be significantly underestimated for structures with fundamental period around the pulse period.

The effect of the directivity pulse embedded in the ground motion on the inelastic response of the structures might also be very significant. For example, Iervolino and Cornell [18] reported that, for periods about half the period of the pulse, the inelastic displacements can be five times larger than the elastic ones; this means that the equal displacement rule does not hold in this range of periods. It appears that, if directivity phenomena are present, the equal displacement rule holds for periods larger than the pulse period [30]. It is noted that the inelastic behavior of structures to various pulses has been the object of interest of several researchers [13, 31]. A common observation is that the inelastic behavior can be very sensitive to multiple parameters, such as the viscous damping and the inelastic model used.

In this section, the effect of the most significant (first detected) directivity pulse inherent in near-fault ground motions on the inelastic response of SDOF structures is investigated. To this end, the predominant pulse embedded in the normal to the fault component of 91 records from the NGA strong motion data base, which were characterized as pulse-like by Baker [7], was identified first, using the

**Fig. 10** Error produced in the maximum inelastic displacement of SDOF structures with  $R_y = 4$  if only the predominant pulse is considered as the base excitation. *Solid red line* shows the mean error for ninety one records, *dashed red lines* show the curves corresponding to the mean error plus/minus one standard deviation



above-mentioned procedure. The corresponding values of the pulse parameters can be found in [32]. For each record, the inelastic response of SDOF structures with varying period is calculated, assuming that the base excitation consists of: (a) the original record; and (b) only the corresponding directivity pulse. This comparison can be extended to additional pulses embedded in the ground motion, but this investigation exceeds the purpose of this chapter.

Indicative results are presented in Fig. 10 for oscillators with periods up to 20 s and strength corresponding to  $R_y = 4$ . It is reminded that the *strength reduction factor*,  $R_y$ , (equivalent to the term *yield behavior factor*,  $q_y$ , used in Eurocode 8 [33]) is defined as

$$R_y = F_e / F_y \quad (22)$$

where  $F_e = ma_e$  is the maximum force for elastic response and  $F_y = ma_y$  is the yielding force of the nonlinear system,  $m$  being the mass of the oscillator and  $a_e$  and  $a_y$  being the corresponding elastic acceleration and yield acceleration, respectively. Note that many typical RC structures are designed for values of  $R_y$  around 4. In the results presented here,  $a_e$  was calculated first for each record and each SDOF oscillator assuming elastic response. Then the inelastic response was calculated assuming that yielding was occurring at acceleration  $a_y = a_e/4$  and that the system possesses a horizontal post-yield branch (elastic – perfectly plastic response without hardening). It is noted that  $a_y$  was calculated only for the original record and this value was used in the calculation of the inelastic response under both the original record and the pulse excitation.

In Fig. 10, the error  $e$  for all records, that is produced in the maximum inelastic displacement if only the predominant pulse excitation is used, is plotted versus the normalized (with respect to the pulse period  $T_p$ ) period of the oscillators,  $T/T_p$ . For each record and each oscillator of period  $T$ , the error was calculated from the relation:

$$e(T) = [d_p(T) - d_{or}(T)] / d_{or}(T) \quad (23)$$

in which  $d_{or}(T)$  is the maximum displacement of the oscillator of period  $T$  under the original record and  $d_p(T)$  the displacement under the corresponding pulse excitation. In Fig. 10, the solid red line shows the mean curve and the dashed red lines show the mean plus/minus one standard deviation curves.

These results show that, on average, the error is less than 20 % for structures with period  $T > 0.6 T_p$ . The minimum error occurs for oscillators with period  $T$  close to  $T_p$  while the mean error is less than 5 % and the mean error plus/minus one standard deviation is no more than 30 % for structures with periods in the range from about  $0.8 T_p$  to about  $1.5 T_p$ . This behavior implies that the directivity pulse governs the inelastic response of structures with period  $T > 0.6 T_p$  since the pulse alone can capture quite well the overall response. On the contrary, the effect of the directivity pulse seems not to be important for structures with period  $T$  less than  $0.5 T_p$ , where the pulse alone underestimates the nonlinear response significantly.

As shown in Fig. 10, the error produced by the first pulse alone is quite large in some cases, even for  $T > 0.6 T_p$ . This happens because the second pulse is important in such cases. It is noted that the first identified pulse is not necessarily the most important one (e.g. in terms of the corresponding energy flux) and there are few cases in which the second pulse is equally or even more important. Additional analyses (not presented here) show that the addition of the second pulse improves the results significantly, reducing the error to acceptable limits for all records and for a larger range of periods.

## 5 Conclusions

A new method for the identification of the directivity pulse embedded in near-fault ground motions is presented. The pulse is mathematically represented by the Mavroeidis and Papageorgiou (M&P) wavelet [13], the parameters of which are determined through a well-defined procedure that is based on several new concepts, specifically:

- The period of the pulse is determined from the peak of the  $S_d \times S_v$  product spectrum for 5 % damping, which is defined as the product of the velocity and the displacement response spectra. It is proven that the  $S_d \times S_v$  product spectrum for zero damping is an adequate envelope of the Fourier amplitude spectrum of the convolution integral of the ground velocity and the ground acceleration.

- The remaining parameters of the wavelet (amplitude, duration and phase shift) are determined from the matching of the targeted spectral amplitudes of the ground motion using a new relationship which is established between the cumulative absolute displacement (*CAD*) of the M&P wavelet and its spectral amplitude.

The proposed method can be extended to the determination of additional pulses inherent in the ground motion. To this end, the detected significant pulse is subtracted from the original record to derive the *residual record*, to which the method is applied for the derivation of the second pulse. This procedure can be repeated several times until all significant pulses are derived. The summation of all significant pulses produces a mathematical representation of the original record.

The new method is applied to ninety-one pulse-like records from the NGA strong motion database in order to investigate the effect of the directivity pulse on the inelastic response of SDOF structures. The investigation is restricted to the effect of the most significant pulse only. Comparison of the inelastic responses produced by the pulse alone with the corresponding one produced by the original record shows that the directivity pulse governs the inelastic response of structures with period  $T > 0.6 T_p$  while its effect seems not to be important for structures with period  $T$  less than  $0.5 T_p$ .

## References

1. Somerville PG (1998) Development of an improved representation of near-fault ground motions. In: Proceedings of SMIP98 seminar on utilization of strong motion data California strong motion instrumentation program Sacramento CA, 1–20
2. Alavi B, Krawinkler H (2000) Consideration of near-fault ground motion effects in seismic design. In: Proceedings of 12th world conference on earthquake engineering, New Zealand
3. Sasani M, Bertero VV (2000) Importance of severe pulse-type ground motion in performance-based engineering: historical and critical review. In: Proceeding of 12th world conference on earthquake engineering, New Zealand
4. Rupakhety R, Sigurdsson SU, Papageorgiou AS, Sigbjornsson R (2011) Quantification of ground motion parameters and response spectra in the near field region. *Bull Earthq Eng* 9:893–930
5. Baker JW (2008) Identification of near-fault velocity pulses and prediction of resulting response spectra. In: Proceeding of geotechnical earthquake engineering and structural dynamics IV, Sacramento CA, 18–22 May 2008
6. Burks LS and Baker JW (2014) Fling in near-fault ground motions and its effect on structural collapse capacity. In: Proceedings of 10th U.S. national conference on earthquake engineering, frontiers of earthquake engineering, Anchorage, Alaska, 21–25 July 2014
7. Baker JW (2007) Quantitative classification of near-fault ground motions using wavelet analysis. *Bull Seismol Soc Am* 97:1486–1501
8. Zhai C, Chang Z, Li S, Chen Z, Xie L (2013) Quantitative identification of near-fault pulse-like ground motions based on energy. *Bull Seismol Soc Am* 103:2591–2603
9. Kardoutsou V, Taflampas I, Psycharis I (2014) A new method for the classification of ground motions as pulse-like or non pulse-like. In: Proceedings of 2nd European conference on earthquake engineering and seismology, Istanbul, Turkey, 25–29 August 2014

10. Beresnev IA, Atkinson GM (1998) Stochastic finite-fault modeling of ground motions from the 1994 Northridge California earthquake. I Validation on rock sites. *Bull Seismol Soc Am* 88:1392–1401
11. Boore DM (2003) Simulation of ground motion using the stochastic method. *Pure appl Geophys* 160:635–675
12. Motazedian D, Atkinson G (2005) Stochastic finite-fault modeling based on a dynamic corner frequency. *Bull Seismol Soc Am* 95:995–1010
13. Mavroeidis GP, Papageorgiou AS (2003) A mathematical representation of near-fault ground motions. *Bull Seismol Soc Am* 93(3):1099–1131
14. Motazedian D, Moinfar A (2006) Hybrid stochastic finite fault modeling of 2003 M6.5 Bam earthquake (Iran). *J Seismolog* 10:91–103
15. Taflanidis AA, Scruggs JT, Beck JL (2008) Probabilistically robust nonlinear design of control systems for base-isolated structures. *J Struct Control Health Monit* 15:697–719
16. Psycharis IN, Fragiadakis M, Stefanou I (2013) Seismic reliability assessment of classical columns subjected to near-fault ground motions. *Earthquake Eng Struct Dynam* 42:2061–2079
17. Shahi S, Baker JW (2011) An empirically calibrated framework for including the effects of near-fault directivity in probabilistic seismic hazard analysis. *Bull Seismol Soc Am* 101(2):742–755
18. Iervolino I, Cornell CA (2008) Probability of occurrence of velocity pulses in near-source ground motions. *Bull Seismol Soc Am* 98(5):2262–2277
19. Shahi SK (2013) A probabilistic framework to include the effects of near-fault directivity in seismic hazard assessment, Ph.D. Dissertation, Stanford University
20. Vassiliou MF, Makris N (2011) Estimating time scales and length scales in pulse-like earthquake acceleration records with wavelet analysis. *Bull Seismol Soc Am* 101(2):596–618
21. Taflampas IM, Spyarakos CC, Koutromanos LA (2009) A new definition of strong motion duration and related parameters affecting the response of medium-long period structures. *Soil Dyn Earthquake Eng* 29(4):752–763
22. Rodriguez-Marek A (2000) Near-fault seismic site response. Ph.D. Dissertation, Department of Civil Engineering, University of California, Berkeley
23. Hudson DE (1979) Reading and interpreting strong motion accelerograms. EERI engineering monographs on earthquake criteria, structural design and strong motion records
24. Daubechies I (1992) Ten lectures on wavelets CMBS-NSF Regional Conference Series in Applied Mathematics. SIAM, Philadelphia (Ch. 3)
25. EPRI (1991) Standardization of the cumulative absolute velocity. EPRI Report RP3096-1, Electric Power Research Institute, Palo Alto, California
26. Zamora M, Riddell R (2011) Elastic and inelastic response spectra considering near-fault effects. *J Earthquake Eng* 15:775–808
27. Arias A (1970) A measure of earthquake intensity. In: Hansen RJ (ed) *Seismic design for nuclear power plants*, MIT Press, Cambridge, MA, pp 438–483
28. Clough RW, Penzien J (1997) *Dynamics of Structures*. McGraw-Hill
29. Baker JW (2014) [http://www.stanfordedu/~bakerjw/pulse-classification\\_old.html](http://www.stanfordedu/~bakerjw/pulse-classification_old.html). (Last visited May 2014)
30. Taflampas I, Psycharis IN (2008) Investigation of the effect of the ground motion characteristics on the  $R_y$ - $\mu$  relation for the inelastic response of SDOF structures. In: 14th world conference on earthquake engineering, Beijing, China, 12–17 October 2008
31. Panagiotou M (2008) Seismic design, testing and analysis of reinforced concrete wall buildings. Ph.D. Dissertation, University of California, San Diego
32. Mimoglou P, Psycharis IN, Taflampas IM (2014) Explicit determination of the pulse inherent in pulse-like ground motions. *Earthquake Eng Struct Dynam* 43:2261–2281
33. European Committee for Standardization (CEN) (2004) Eurocode 8: design of structures for earthquake resistance. EN 1998, Brussels

Computational Methods in Earthquake Engineering  
Volume 3

Papadrakakis, M.; Plevris, V.; Lagaros, N.D. (Eds.)

2017, X, 418 p. 182 illus., Hardcover

ISBN: 978-3-319-47796-1